Key Engineering Materials
ISSN: 1662-9795, Vol. 926, pp 481-498
doi:10.4028/p-hf76i3

Submitted: 2021-12-17
Revised: 2022-01-24
Accepted: 2022-01-28
Online: 2022-07-22

A Model for Roll-Drawing of Full Sections with Experimental Verification

Rolf Braun[1,a*], Ilham Zuhdi Ananta[1,b], Gilar Bagaskoro Buono[1,c], Christian Overhagen[1,d] and Mayeen Uddin[1,e]

[1]University of Duisburg-Essen, Chair of Metallurgy and Metal Forming, Friedrich-Ebert-Str. 12, 47119 Duisburg, Germany

[a]rolf.braun@uni-due.de, [b]ilham.ananta@stud.uni-due.de, [c]gilar.buono@stud.uni-due.de, [d]christian.overhagen@uni-due.de, [e]mayeen.uddin@stud.uni-due.de

Keywords: roll-drawing, flat wire, full sections drawing, forward-slip, roll-drawing force, roll separating force, lateral spread, width of contact area, local area, free side-surface.

Abstract. Roll-drawing of full sections is an alternate process for wire drawing through a closed die, as it conserves less hard tool materials. It therefore enhances the resource efficiency of thin wire production. As the tools are rotating, the relative velocity is lower and friction is reduced. Apart from this, there is only little knowledge about the process mechanics inside the deformation region. According to the relative motion mentioned above, a neutral point should exist within the deformation region, but this hypothesis is unconfirmed until today. In the present work, a combination of an improved empirical model for the lateral spread in roll-drawing and a mechanical model for roll drawing based on the slab method is proposed. The mechanical model deviates from the well-known rolling theory by the fact that a zero deformation torque should exist on the rolls, it predicts the neutral angle, the forward-slip, the external drawing force and the roll separating force. The hypothesis of existence of a neutral point in the deformation region is supported by experimental measurements of the nonzero forward slip in the roll-drawing process. Measurement is done on copper wire, where 200 passes with initial round section sizes ranging from 2 mm to 1.3 mm with an increment of 0.1 mm are evaluated.

Introduction

The roll-drawing process with its characteristic could be a step towards an energy and material efficient production of full-sections, as less hard tool materials and energy is consumed. But compared to the cold rolling process, only few researchers have published knowledge, which can enhance the process planning on industrial level. Especially with respect to the pass design for the roll-drawing process there is a lack of precise spread formulas, but some formulas were proposed in former time [1, 2, 3]. In the mentioned resources, researchers have observed that the material spread behavior in roll-drawing of carbon steel is quite different to the one observed in hot and cold rolling. For the efficient design of drawing machines and their electrical drive systems, additional process and control models specialized for the roll-drawing process would be helpful. When a pass design for the production of a new full-section has to be developed, one of the first questions is about which initial section has to be taken and additional which force, torque, and power demand can be expected. Often, previously hot rolled round wire rod serves as an initial section for the production of smaller cold drawn full-sections. For the calculation of the groove size and its filling in regular and irregular passes, there in conjunction with an equivalent flat pass method, a precise empirical spread formula is a valuable help to come to a first design. According to that, the passes round to flat and the succeeding flat to flat pass are identified as model passes and investigated in this work. Two new spread formulas are proposed by the authors. For the calculation of force, torque, and power demand of the drives a fast mechanical model for roll-drawing based on the slab method is also proposed in the next sections. For investigation of the lateral spread in roll-drawing, and for the experimental verification of the mechanical model, copper wire (Cu-ETP) is chosen.

Nomenclature

A, B, C, D, E, F, G	**parameters of the spread equations**	**k(x), p(x)**	coefficients of the ordinary differential equation
a_p , b_p , c_p , d_p	parameters of the flowcurve	$\mathbf{k_f}$	flow stress
$\mathbf{A_x}$	**local cross section area**	$\mathbf{k_{RS}}$	**scalar influencing factor of free-side surface evolution**
$\mathbf{A_{x>0}}$	wire cross section in a distance after the exit plane of the roll gap	$\mathbf{l_d}$, $\mathbf{l_{dx}}$	length under direct pressure, local length under direct pressure
$\mathbf{A_{CS}}$	circular section of the flattened wire	$\mathbf{T_B}$	torque from friction in the bearing
$\mathbf{a_S}$	inner length of circular section	$\mathbf{T_D}$	virtual torque from drive
$\mathbf{b_0}$, $\mathbf{b_1}$, $\mathbf{b_x}$	initial width of wire, final width of wire, local width of wire	$\mathbf{T_R}$	**rolling torque in the roll gap**
$\mathbf{b_{max}}$, $\mathbf{b_{max\,x}}$	width of wire, local width of wire	$\mathbf{T_T}$	torque from drawing force
$\mathbf{b_{min}}$, $\mathbf{b_{min\,x}}$	minimum width / width of contact area, local minimum width	$\mathbf{R_B}$	radius of bearing
$\mathbf{b_{x>0}}$	width of wire in a distance after the exit plane of the roll gap	$\mathbf{R_R}$	radius of roll
$\mathbf{\Delta b}$	absolute spread / absolute change in width	$\mathbf{R_{S0}}$	initial side radius of wire
$\mathbf{d_0}$	initial diameter of wire	$\mathbf{R^2}$	coefficient of determination
$\mathbf{d_S}$	outer length of circular section	$\mathbf{v_0}$	inlet wire velocity
$\mathbf{d_R}$	diameter of roll	$\mathbf{v_1}$	exit wire velocity
$\mathbf{F_B}$	force acting in the bearing	$\mathbf{v_x}$	local longitudinal component of wire velocity
$\mathbf{F_{RS}}$	roll separating force	$\mathbf{v_{cR}}$	circumferential velocity of roll
$\mathbf{F_T}$	drawing force	$\mathbf{v_{xR}}$	local longitudinal component of roll velocity
$\mathbf{h_0}$, $\mathbf{h_1}$	initial height of wire, final height of wire	$\mathbf{x_N}$	position of the neutral point
$\mathbf{\Delta h}$	abs. reduction / abs. change in height	**x, y, z**	cartesian coordinates

Nomenclature

Nomenclature

α	contact angle	μ_B, μ_R	coefficient of friction bearing, coefficient of friction roll gap
α_N	neutral angle	$\bar{\mu}$	general friction coefficient
β	degree of spread	σ_N	normal stress
$\varepsilon_h = \Delta h / h_0$	related change in height	σ_x, σ_y	principal stresses
κ	forward slip	τ	shear stress
λ_{ext}	external plastic stretch	φ	logarithmic true strain
μ	coefficient of friction		

Experimental Procedure

Spread in the initial Pass: Round-Flat. The initial pass is done on samples prepared in advance by classical cold drawing of 8 mm hot rolled copper wire (Cu-ETP) through static converging dies. Cu-ETP is an electrolytic refined copper, which contains at least 99.90 % copper (Cu), has maximum contents of oxygen(O) 0.04 %, bismuth (Bi) 0.0005 % and lead (Pb) 0.005 %. The material has a yield strength of 120 MPa, ultimate tensile strength of 230 MPa and a fracture elongation of 35 % in the as-received condition. The drawing of the wire down to the initial sizes for the roll-drawing procedure leads to diameters ranging from 2 mm down to 1.3 mm, with an increment of 0.1 mm. The wire is not annealed after that preparation. In the succeeding roll-drawing procedure, see Fig. 4 a) left, the related reduction in height εh is increased from a minimum reduction per pass of 5 % to a maximum of 50 % per pass. For each reduction one sample of each prepared initial diameter is used. The related reduction in height εh is increased from sample to sample by an increment of 5 %. After the pass, each resulting sample height h1 and maximum width b1 is measured. For all samples, the same set of rolls is used. The roll diameter dR of the roller-die attached to the chain driven drawing machine is 42 mm, see Fig.1. To prevent diagonal rolling during the roll-drawing process, the samples are centered to the roll gap by a roller guide fixed close to the inlet plane. The roll gap is adjusted by means of a mechanical spindle.

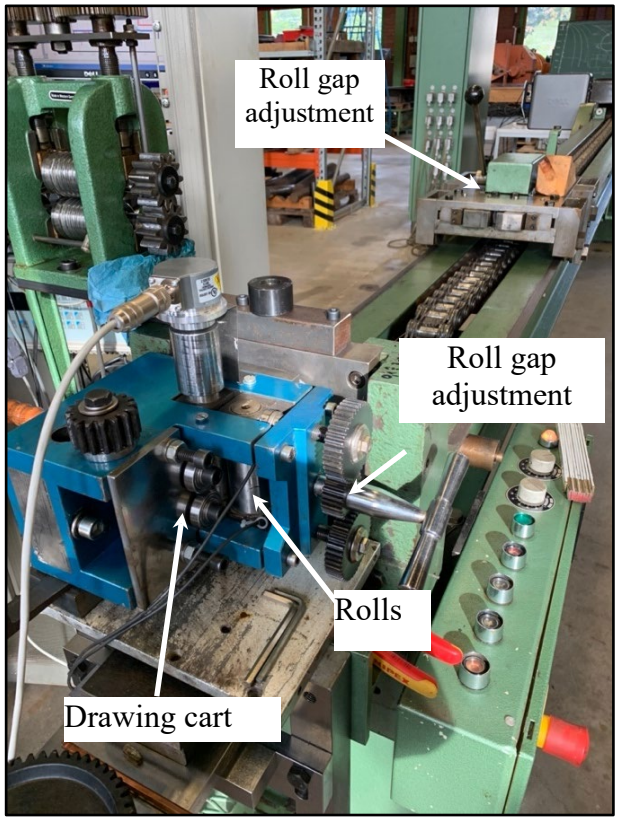

Fig. 1: Roller-die, roll diameter d_R = 42 mm

Spread in the second Pass: Flat-Flat. From the set of samples with eight different initial diameters which are deformed by the first pass in the first experiment, see Fig. 4 a) left, the ones with 1.3 mm, 1.6 mm and 2 mm initial diameter are picked out for a further investigation in a second pass. On the samples with deformation from the preceding first round to flat pass, an additional reduction in that second pass is done, see Fig. 4 a) right. Increments of 10 % for the related reduction in height of the first pass and of 5 % for the following second pass are taken. After the first pass, the resulting height, as well as the resulting maximum width, is measured. These values represent the initial sample sizes for the second pass. After the second pass, the final dimensions height and maximum width are measured. In between the first and second pass, the samples are not annealed.

Measurement of roll-drawing force, roll separating force and forward slip: Round-Flat. For the experimental verification of the mechanical model for the calculation of roll-drawing force FT, roll separating force FRS and forward slip κ in roll-drawing measurements are taken. The longitudinally applied roll-drawing force is measured by a load cell clamped between the free end of the wire at the exit of the roll gap and the drawing cart. The roll separating force is measured by load cells placed under the bearing chocks. For the forward-slip measurement, one encoder is attached to the bottom roll for measurement of the roll circumferential speed vcR. The speed of the drawing cart, which is set to be equal to the exit speed of the wire v1, is measured by a second encoder. The roll-drawing is conducted on two different states of the copper wire. One set of data is recorded in an experiment conducted with work hardened copper wire and another set with copper wire which has been recrystallized at a temperature of 450 °C for a time of 30 min at atmosphere.

Measurement of flow stress. For the verification of the mechanical model, a flow curve of the copper in recrystallized state is needed. For this purpose are taken samples of 6.2 mm in diameter which are recrystallized at a temperature of 450 °C for a time of 30 min at atmosphere. These samples are upset in a compression test to the extent of the logarithmic true strain φ equal to 1.16. For stress and strain calculation the acting force and the travel of the upsetting tool is recorded.

Mathematical Method

Lateral spread calculation in roll-drawing: For calculation of lateral spread in the roll-drawing process only some formulas are published, most of them are having their roots in the hot-flat rolling. The spread formula of Hill [5] is given as Eq. 1. Jaschke [1] is using the formula of Hill with the coefficient 0.525 instead of 0.5 which has been proposed by Limant [4], additionally he is using the final width b1 on the right-hand side of the equation instead of initial width b0, see Eq. 2. The length under direct pressure ld is calculated with Eq. 3:

$$\beta_{Hi} = \frac{b_1}{b_0} = \left(\frac{h_0}{h_1}\right)^{0.5\cdot\exp\left(-0.5\cdot\frac{b_0}{l_d}\right)} . \tag{1}$$

$$\beta_{Ja} = \frac{b_1}{b_0} = \left(\frac{h_0}{h_1}\right)^{0.5\cdot\exp\left(-0.525\cdot\frac{b_1}{l_d}\right)} . \tag{2}$$

$$l_d = \sqrt{R_R \cdot \Delta h} = \sqrt{R_R \cdot \left(h_0 - h_1\right)} . \tag{3}$$

Lambiase [3] proposed for the prediction of the degree of spread β in roll-drawing Eq. 4 for steel samples he investigated, where the initial wire diameters d0 were 4.6 mm and 5.3 mm and the diameter of the idle rolls dR 80 mm.

$$\beta_{La} = \frac{b_1}{b_0} = 1.02 \cdot \left(\frac{h_0}{h_1}\right)^{0.45} - 0.29 \cdot h_0^{-1.6} \cdot \left(\frac{h_0}{h_1}\right)^{3.1} . \quad (4)$$

For the prediction of spread in roll-drawing of copper wire, two new equations are proposed by the authors. For the first pass, forming the round section to the flat shape with curved side surface Eq. 5 and for the second pass forming the flat into a flat Eq. 6 is proposed.

$$\beta_{An} = \frac{b_1}{b_0} = \left(\frac{h_0}{h_1}\right)^{A \cdot \exp(-B \cdot \frac{b_1}{l_d})} - C \cdot h_0^{-D} \cdot \left(\frac{h_0}{h_1}\right)^{E} . \quad (5)$$

$$\beta_{Bu} = \frac{b_1}{b_0} = A \cdot \left(\frac{h_0}{h_1}\right)^{B} - C \cdot h_0^{-D} \cdot \left(\frac{h_0}{h_1}\right)^{E} + \left(\frac{h_0}{h_1}\right)^{F \cdot \exp(-G \cdot \frac{b_0}{l_d})} . \quad (6)$$

Calculation of roll-drawing force, roll separating force and forward slip: Round-Flat pass. For the prediction of the necessary force, torque and power demand of a drawing machine used for the roll-drawing process a mechanical model based on the slab method is given in the following section, for flat wire production and flat rolling, such type of models are known [6, 7]. The main geometrical dependencies in the roll gap are derived with the help of Fig. 2. The acting stresses and geometric properties of the infinitesimal slab element, which are relevant to form the equilibrium of forces, are shown in Fig. 3. In Fig. 4 b) the geometric properties for the model of the local cross- section area Ax of the wire in the gap are shown. Considered is the symmetric case with respect to friction coefficient μ as well as the idle roll radius of top RRt and bottom roll RRb.

The equations Eq. 7 to Eq. 11 describe the geometrical relations in the roll gap. With the position dependent height h_x from Eq. 10 the position dependent maximum true strain φ in height direction is calculated, given in Eq. 12.

$$\sin(\alpha) = \frac{-x}{R_R} . \quad (7)$$

$$\cos(\alpha) = \sqrt{1 - \sin(\alpha)^2} . \quad (8)$$

$$\tan(\alpha) = \frac{\sin(\alpha)}{\cos(\alpha)} . \quad (9)$$

$$h_x = h_1 + 2 \cdot R_R \cdot (1 - \cos(\alpha)) . \quad (10)$$

$$\frac{dh_x}{dx} = -2 \cdot \tan(\alpha) . \quad (11)$$

$$\varphi = \ln(\frac{h_0}{h_x}) . \quad (12)$$

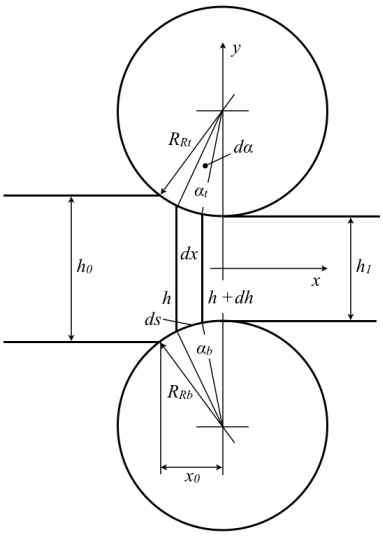

Fig. 2: Roll gap geometry.

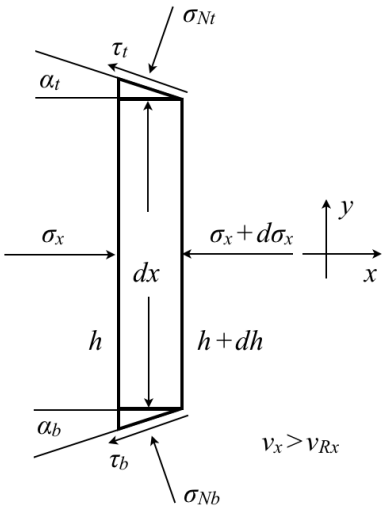

Fig. 3: Stresses acting on the infinitesimal slab in the forward slip zone.

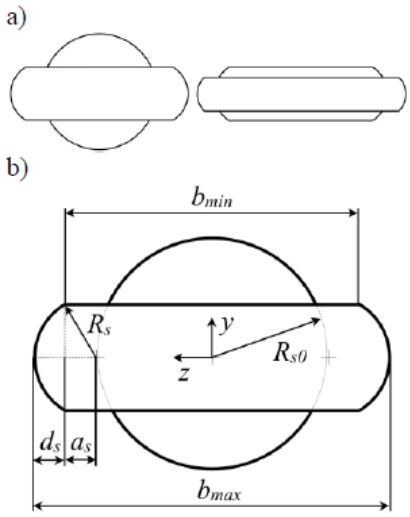

Fig. 4: a) Initial round to flat pass, second flat to flat pass. b) Geometry of local area A_x and wire dimensions.

With Eq. 13 a local representation of the length under direct pressure l_{dx} is calculated, which is necessary for the calculation of the local maximum width b_{max} along the roll gap coordinate x, represented by Eq. 14. The local distribution or evolution of the shape of the free-side surface along the roll gap is modeled with Eq. 15. The scalar value k_{RS} is dependent on the reduction in the pass. The evaluation of the k_{RS} value is described in a later section. For the calculation of the position dependent width of contact area $b_{min\,x}$ from the position dependent maximum width b_x and with the help of the shape of the free-side surface, described by the radius of the free-side surface R_{Sx}, the inner length a_S and the outer length d_S of the circular section have to be calculated in advance. The local area A_x at each position in the roll gap is subdivided into a center part of rectangular shape and two circular sections A_{CS} on the sides, see Eq. 20.

$$l_{dx} = \sqrt{R_R \cdot (h_0 - h_x) - \left(\frac{h_0 - h_x}{2}\right)^2} \,. \tag{13}$$

$$b_x = b_0 \cdot \left(\frac{h_0}{h_x}\right)^{0.5 \cdot \exp(-0.5 \cdot \frac{b_0}{l_{dx}})} \,. \tag{14}$$

$$R_{Sx} = -\left(\frac{b_x - b_0}{b_1 - b_0}\right) \cdot k_{RS} + R_{S0} \,. \tag{15}$$

$$a_S = R_{Sx} \cdot \cos\left(\sin^{-1}\left(\frac{h_x}{2 \cdot R_{Sx}}\right)\right) \,. \tag{16}$$

$$d_S = R_{Sx} - a_S \,. \tag{17}$$

$$b_{\min x} = b_x - 2 \cdot d_S \,. \tag{18}$$

$$A_{CS} = 0.5 \cdot \left(2 \cdot R_{Sx}^2 \cdot \sin^{-1}\left(\frac{h_x}{2 \cdot R_{Sx}}\right) - h_x \cdot a_S\right) \,. \tag{19}$$

$$A_x = b_{\min x} \cdot h_x + 2 \cdot A_{CS} \,. \tag{20}$$

The force equilibrium on the slab in *x*-direction is represented by Eq. 21, which is derived from the acting stresses given in Fig. 3. After canceling out the width *b* and a bit of rearrangement one comes to Eq. 22. For the following formulas, a general friction coefficient $\overline{\mu}$ is defined, where the positive sign has to be used in the forward-slip zone and the negative sign in the backward-slip zone, see Eq. 23. With Coulomb's friction law, Eq. 24, and the force equilibrium on the slab in *y*-direction, Eq. 25, the horizontal stress σ_x and the vertical stress σ_y are linked. For the description of the normal stress in *y*-direction as a function of the longitudinal normal stress, Tresca's yield criterion is used in the given way, see Eq. 27. Following some further rearrangement, Eq. 28 is formed. By placing the appropriate signs in front of the friction coefficient, for forward and backward-slip zone, in Eq. 29 and Eq. 30 one comes to the two differential equations, one valid for the region in front of the neutral point and one for the region behind.

$$0 = \sigma_x \cdot h \cdot b - (\sigma_x + d\sigma_x) \cdot (h + dh) \cdot b - \sigma_N \cdot 2 \cdot \sin(\alpha) \cdot \frac{dx}{\cos(a)} \cdot b - \tau \cdot 2 \cdot \cos(\alpha) \cdot \frac{dx}{\cos(a)} \cdot b \,. \tag{21}$$

$$0 = h \cdot \frac{d\sigma_x}{dx} + \sigma_x \cdot \frac{dh}{dx} + 2 \cdot \sigma_N \cdot \tan(\alpha) + 2 \cdot \tau \,. \tag{22}$$

$$\overline{\mu} = \pm \mu \,. \tag{23}$$

$$\tau = \overline{\mu} \cdot \sigma_N \,. \tag{24}$$

$$0 = \sigma_y \cdot dx \cdot b - \sigma_N \cdot \cos(\alpha) \cdot \frac{dx}{\cos(\alpha)} \cdot b + \tau \cdot \sin(\alpha) \cdot \frac{dx}{\cos(\alpha)} \cdot b \,. \tag{25}$$

$$\sigma_N = \frac{\sigma_y}{1 - \overline{\mu} \cdot \tan(\alpha)} \,. \tag{26}$$

$$k_f = \sigma_y - \sigma_x \,. \tag{27}$$

$$\frac{d\sigma_x}{dx} = p(x) \cdot \sigma_x + k(x) \,. \tag{28}$$

$$p(x) = -\frac{2}{h_x} \cdot \frac{\overline{\mu} \cdot (1 + \tan^2(\alpha))}{1 - \overline{\mu} \cdot \tan(\alpha)} \,. \tag{29}$$

$$k(x) = -\frac{2}{h_x} \cdot \frac{\overline{\mu} + \tan(\alpha)}{1 - \overline{\mu} \cdot \tan(\alpha)} \cdot k_f(\phi) \,. \tag{30}$$

The solution of the differential equation in *x*-direction is leading to the longitudinal stress distribution in the roll-gap, $\sigma_{x\,(x)}$, from which with the help of Eq. 27 and Eq. 43 the vertical stress distribution $\sigma_{y\,(x)}$ in the gap can be calculated. By integration of the product of the vertical stress distribution $\sigma_{y\,(x)}$ and a mean value of the width of contact area $b_{min\,x}$ and the maximum local width b_x along the gap coordinate *x* the roll separating force F_{RS} is calculated, see Eq. 31. For the resulting rolling torque in the roll gap T_R the quite similar formula, Eq. 32, is derived.

$$F_{RS} = \int_0^{x0} \frac{\sigma_y(x)}{\cos(\alpha)} \cdot \frac{b_{\min x} + b_x}{2} dx \quad . \tag{31}$$

$$T_R = R_R \cdot \int_0^{x0} \frac{\tau(x)}{\cos(\alpha)} \cdot \frac{b_{\min x} + b_x}{2} dx \quad . \tag{32}$$

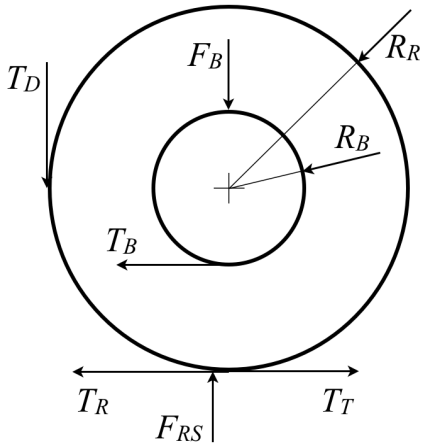

Fig. 5: Torques and forces acting on the roll.

In Fig. 5 the different torques acting on the roll are shown. There is the rolling torque T_R, the bearing torque T_B as a result of the friction acting in the bearing, the external torque T_T coming from the application of the drawing force which can be described also by a stress acting on the cross-section area of the wire in the exit plane of the roll gap and an additional virtual torque from an external drive T_D. These four torques have to be in equilibrium, which is represented by Eq. 35. For the roll-drawing case, the external torque from a drive T_D has to become to zero.

$$T_B = F_{RS} \cdot \mu_B \cdot R_B \quad . \tag{33}$$

$$T_T = \frac{\sigma_{x=0} \cdot A_{x=0}}{2} \cdot R_R \quad . \tag{34}$$

$$T_D = T_R + T_B - T_T \quad . \tag{35}$$

The following equations Eq. 36 and Eq. 37 are describing the longitudinal component of the roll circumferential speed v_{xR} and the longitudinal speed of the drawn wire v_x at each position in the roll gap.

$$v_{xR} = v_{cR} \cdot \cos(\alpha) \quad . \tag{36}$$

$$v_x = \frac{A_{x=xN}}{A_x} \cdot v_{cR} \cdot \cos(\alpha_N) \quad . \tag{37}$$

The forward-slip is defined by Eq. 38. A stretching of the material after the roll gap can be identified by the value of the degree of stretch λ_{ext} deviating from one. The external plastic stretch λ_{ext} is calculated with Eq. 39, where the measured drawing velocity v_{1ms} is related to the calculated velocity $v_{x=0}$ of the wire at the exit of the gap. The influence of such an external plastic stretch on the cross-section of the wire $A_{x>0}$ measured in some distance to the exit plane of the roll gap is calculated with Eq. 40. The influence of such an external stretch on the wire dimensions, maximum width $b_{x>0}$

and minimum width $b_{min(x>0)}$, measured in some distance to the exit plane of the gap is considered by Eq. 41 and Eq. 42.

$$\kappa = \frac{v_1 - v_{cR}}{v_{cR}} \cdot 100\% \quad . \tag{38}$$

$$\lambda_{ext} = \frac{v_{1ms}}{v_{x=0}} \quad . \tag{39}$$

$$A_{x>0} = \frac{A_{x=0}}{\lambda_{ext}} \quad . \tag{40}$$

$$b_{x>0} = \frac{A_{x>0} - 2 \cdot A_{CS(x=0)}}{h_{x=0}} + 2 \cdot d_{S(x=0)} \quad . \tag{41}$$

$$b_{\min(x>0)} = b_{x>0} - 2 \cdot d_{S(x=0)} \quad . \tag{42}$$

Flow curve evaluation for the verification of the mechanical model. On basis of a least squares method, the parameters of the given model function for the cold flow curve, Eq. 43, of the copper wire used in the experiments are evaluated. The true stress k_f is here only a function of the logarithmic true strain φ.

$$k_f(\phi) = a_p \cdot \exp(b_p \cdot \phi) + c_p \cdot \exp(d_p \cdot \phi) \quad . \tag{43}$$

Results and Discussion

Lateral spread calculation in roll-drawing: For the prediction of the lateral spread of copper flat wire in a first pass where an initial round is formed into a flat with curved side-surface, the above proposed Eq. 5 is used, for the investigated range of initial diameters. Eight sets of five free model parameters *A* to *E* have been calculated by a least squares method. The parameters belonging to the different initial diameters d_0 as well as the resulting R^2 values can be seen in Table 1. As examples for the correlation between predicted and measured width values the diagrams in Fig. 6 and Fig. 7 are given, shown are the results for 1.6 mm and 2.0 mm initial wire diameter. The behavior of the copper wire in roll-drawing is in general comparable to what Lambiase [3] has observed with carbon steel wire samples having bigger initial dimensions. Some of the parameters *A* to *E*, like for example parameter *D* is nearly constant for the whole range of initial wire diameters d_0 whereas others, like parameter *B* is strongly fluctuating. But with respect to the overall good R^2 values, one can rely on the calculated final width values. A small drawback is the fact that for the calculation of the final width b_1 with Eq. 5 a numerical solution method has to be used.

Table 1: Parameters for the prediction of the degree of spread in the round to flat pass with the proposed Eq. 5.

d_0 [mm]	A	B	C	D	E	R^2
2,00	0,5645	0,4222	0,0194	1,6538	4,8650	0,983
1,90	0,5135	-0,1360	0,0538	1,6577	3,7878	0,987
1,80	0,5037	-0,0512	0,0461	1,6493	3,5352	0,993
1,70	0,4158	-0,3423	0,0351	1,6487	3,7388	0,975
1,60	0,5492	0,0242	0,0416	1,6394	3,6623	0,990
1,49	0,6285	0,0649	0,0504	1,6332	3,5718	0,990
1,40	0,5634	-0,1046	0,0377	1,6301	3,7822	0,982
1,29	0,6071	-0,0207	0,0366	1,6223	3,6679	0,990

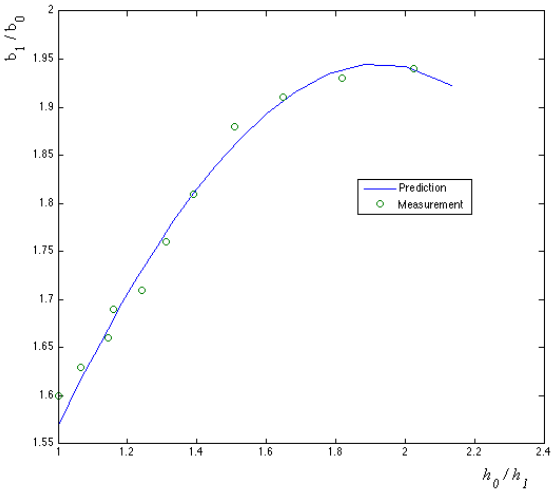

Fig. 6: Predicted and measured degree of spread for 1.6 mm initial sample diameter, *R2* = 0.99.

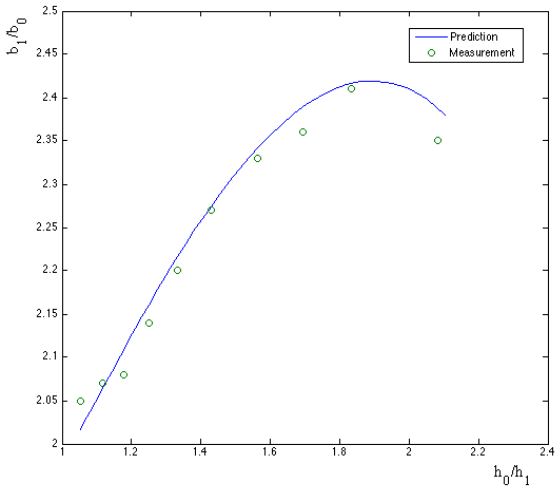

Fig. 7: Predicted and measured degree of spread for 2.0 mm initial sample diameter, *R2* = 0.983.

For the prediction of lateral spread in roll-drawing where a preformed flat is further deformed in a second pass in a flat to flat fashion, the above proposed Eq. 6 can be taken. The results for the seven model parameters *A* to *G*, to be used in conjunction with Eq. 6 and the resulting R^2 values are shown in Table 2. As examples for the quality of the prediction, the plots for the sample sizes with initial height of 1.81 mm and initial width of 2.04 mm out of the 2 mm initial diameter set of samples and the results for the sample with the initial height of 0.95 mm and initial width of 1.95 mm from the 1.6 mm initial diameter set of samples are shown in Fig. 8 and Fig. 9.

Table 2: Parameters for the prediction of the degree of spread in the flat to flat pass with the proposed Eq. 6.

d_0 [mm]	2,00								
h_0 [mm]	**b_0 [mm]**	**A**	**B**	**C**	**D**	**E**	**F**	**G**	**R^2**
1,81	2,04	0,0949	0,5825	0,2337	1,6059	3,0476	1,0353	0,5332	0,996
1,60	2,15	0,0797	0,5600	0,1877	1,6170	2,8291	0,6524	-0,0223	0,991
1,38	2,30	0,0976	0,5781	0,1538	1,6134	3,0084	0,8463	0,4618	0,992
1,17	2,41	0,1000	0,5991	0,1253	1,6072	2,9124	0,7059	0,3463	0,957
0,96	2,39	0,0624	0,5617	0,0477	1,5977	2,8033	0,4176	0,4518	0,956
d_0 [mm]	1,60								
h_0 [mm]	**b_0 [mm]**	**A**	**B**	**C**	**D**	**E**	**F**	**G**	**R^2**
1,44	1,64	0,0744	0,5153	0,1024	1,6202	3,1326	1,1665	1,2410	0,985
1,25	1,74	0,1474	0,6705	0,1985	1,6087	3,0626	1,1106	0,3784	0,992
1,11	1,86	0,0786	0,5949	0,0923	1,6055	2,7870	0,4910	-0,1572	0,956
0,95	1,95	0,0825	0,5437	0,0496	1,5971	2,7911	0,4634	0,5831	0,878
0,86	2,00	0,0912	0,5427	0,0752	0,9471	2,7820	0,6605	0,4495	0,904
d_0 [mm]	1,30								
h_0 [mm]	**b_0 [mm]**	**A**	**B**	**C**	**D**	**E**	**F**	**G**	**R^2**
1,16	1,33	0,1259	0,6062	0,1720	1,6070	2,9707	1,0890	0,2659	0,989
1,04	1,40	0,2045	0,6938	0,1380	-8,3966	3,0491	1,4737	0,6063	0,983
0,92	1,50	0,1451	0,5963	0,1181	1,6086	2,8935	0,9021	0,3110	0,958
0,78	1,61	0,1215	0,5939	0,0743	1,5860	2,7875	0,7404	0,3155	0,910
0,64	1,64	0,0766	1,9233	0,0240	1,5737	8,0398	5,8511	1,8239	0,901

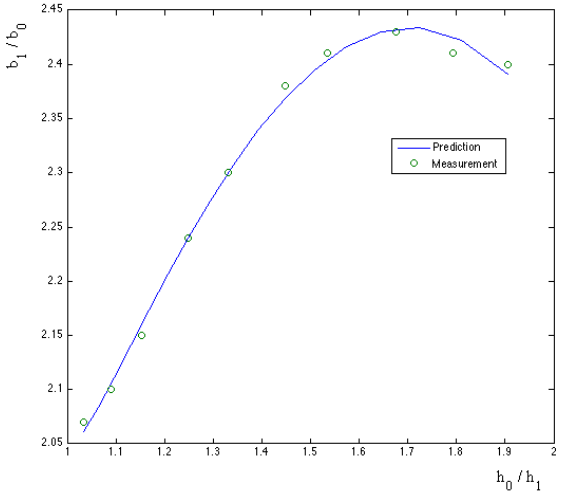

Fig. 8: Predicted degree of spread and measured degree of spread for the sample with 1.81 mm initial height, R2 = 0.996.

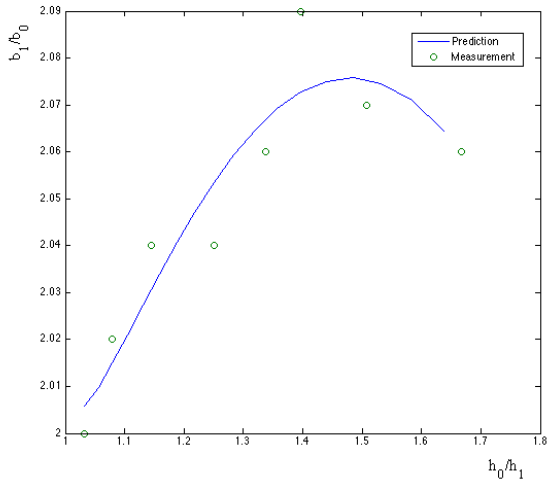

Fig. 9: Predicted degree of spread and measured degree of spread for the sample with 0.95 mm initial height, *R2* = 0.878.

The accuracy of the prediction of lateral spread with Eq. 6 for the flat to flat roll-drawing pass of copper wire is quite high. Even the worst parameter set, with respect to the R^2 value, is capable to describe the general spread behavior. Eq. 6 has, compared to Eq. 5 the benefit, that it can be used for fast calculation on a simple pocket calculator.

Calculation of roll-drawing force, roll separating force and forward slip: Round-Flat pass. For the prediction of roll-drawing force F_T, roll separating force F_{RS} and the forward-slip κ in roll-drawing with the proposed model and its validation roll-drawing experiments on recrystallized copper are conducted. The recrystallized copper is chosen to have a known initial state with respect to the present flow stress k_f of the material. The strain dependent flow stress is evaluated from a compression test. In Fig. 10 the flow stress k_f approximated by an exponential function is plotted over the

logarithmic true strain φ. Results from conducted roll-drawing passes are shown in the following section. As the initial section a 2 mm round wire serves, which is deformed to four different heights h_1, always starting from the initial round section. The measured final dimensions are given in Table 3. The graphical representations of the results, for the different parts of the proposed model are exemplarily given for the second reduction in height.

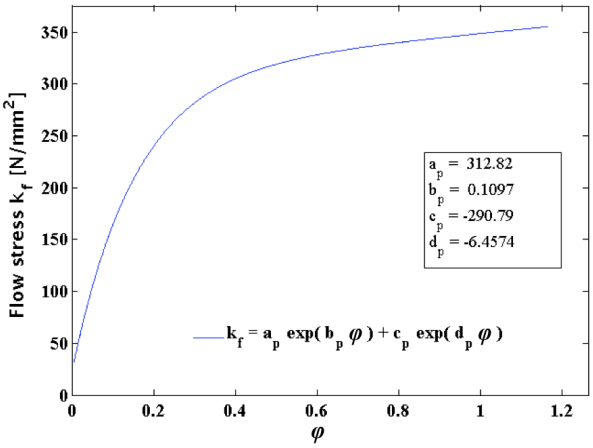

Fig. 10: Flow stress k_f measured in a compression test and approximated by an exponential function, dependent on logarithmic true strain φ, $R_2 = 0.997$.

Table 3: Initial height h_0, initial width b_0, final height h_1 and final width b_1 of four passes.

h_0 [mm]	**b_0 [mm]**
2,00	2,00
h_1 [mm]	**b_1 [mm]**
1,88	2,02
1,79	2,05
1,69	2,09
1,57	2,14

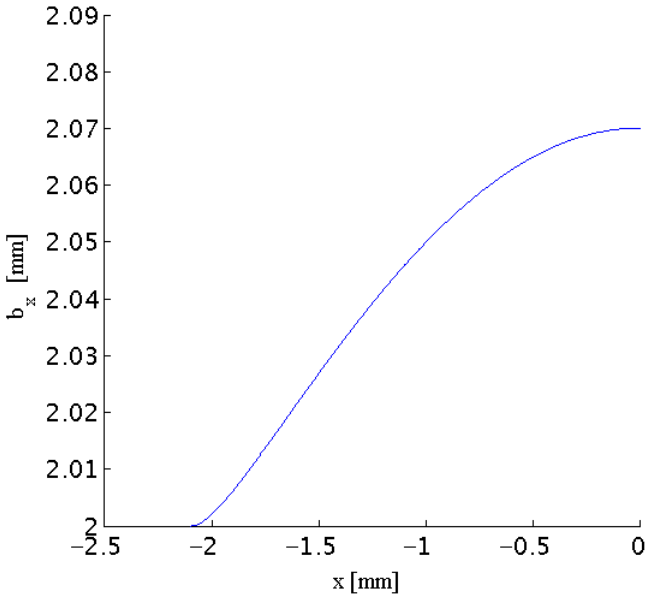

Fig. 11: Representation of the position dependent local maximum width b_x.

In the model, the knowledge about the local area A_x is crucial. It is composed of the rectangular center part and the two curved side parts, remember Fig. 4. At first the local maximum width b_x is calculated, the result is shown in Fig. 11. For the calculation of the area of the curved side parts and for the calculation of the local minimum width $b_{min\,x}$ the side radius R_S has to be known, which is modeled by Eq. 15. In roll pass design practice, for calculation of groove filling in hot rolling operations, it is often the case that this side radius is set to be constant and a parallel shift along with the maximum width is performed which leads to good results. Here it would lead to quite big error on the resulting local area A_x, which can be seen from Fig. 12, where the local area is shown as a function of the local free side-surface radius R_{Sx}. The uppermost line shows the case where the side radius R_S is set equal to the initial radius of the wire R_{S0} and kept constant over the whole length of the roll gap. It can be

seen that this would lead to an increase of area even with respect to the cross-section at the exit of the gap. A question is how the change of the side radius along the contact length happens, in other rolling experiments conducted by the authors, on bigger sample sizes, it has been observed that the change of the side radius R_{Sx} is non-linear along the gap coordinate x but shows a quasi linear dependency with respect to the local absolute change in width Δb_x. That is assumed to be also the case for the roll-drawing. To which extent that change of the shape of the free side-surface is acting, can be described by the scalar influencing factor k_{RS}, see Eq. 15. As an indication for a reasonable choice of the value of influencing factor k_{RS} the plot of the resulting minimum width b_{min} on the exit side of the gap can be used, see Fig. 13. For the model validation measurements of the minimum width b_{min} at the final sections are done by taking close up photograph of the wire top surface and relating the counted number of pixels to real world dimensions. The applied values for k_{RS} and the values of the resulting minimum width b_{min} from the model calculation at the exit plane of the roll gap are collected in Table 4.

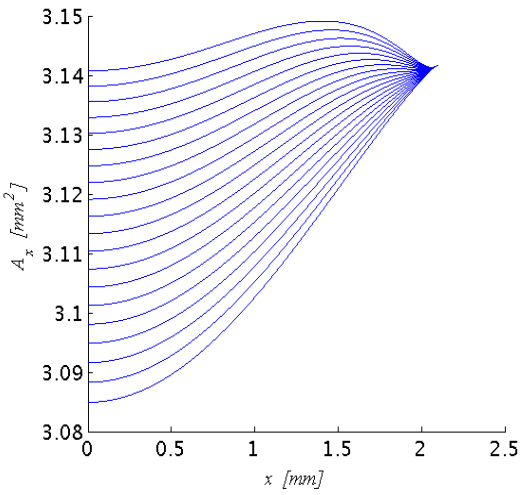

Fig. 12: Different local area *Ax* distributions as a result of different influencing factors kRS in the calculation of the local dependent radius RSx of the free side-surface.

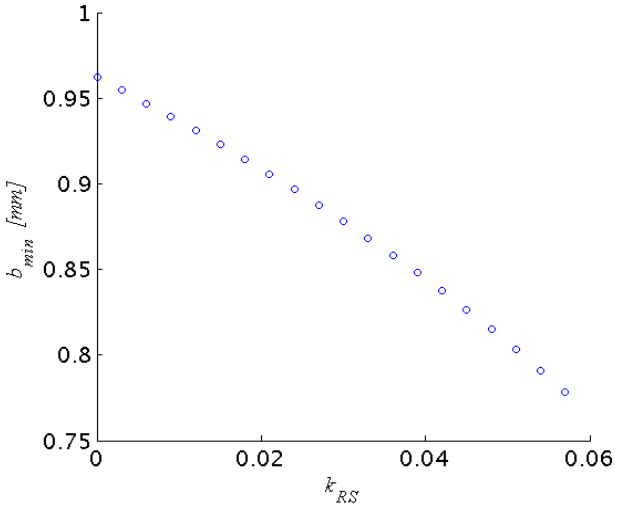

Fig. 13: Final minimum width *bmin* as a function of the scalar influencing factor *kRS* for the calculation of the local side radius *RSx* of the free side- surface.

Table 4: Applied *kRS* values and resulting minimum width values *bmin* at the exit plane of the roll gap of the treated four passes.

k_{RS}	**b_{min} [mm]**
0,0200	0,628
0,0360	0,858
0,0975	0,946
0,1360	1,175

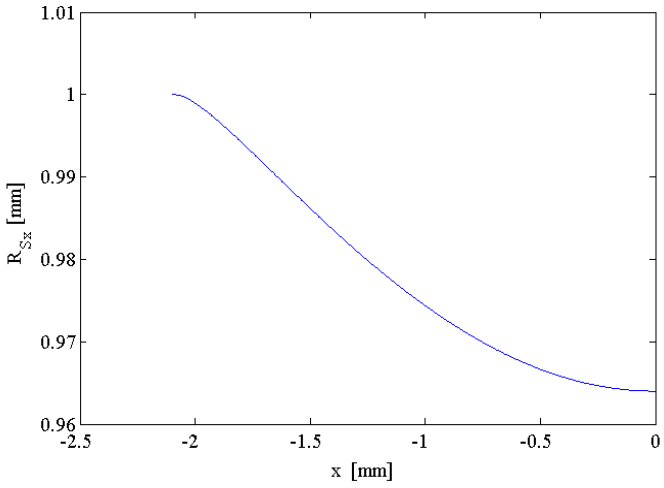

Fig. 14: Local side radius *RSx* of free side-surface calculated with the scalar influencing factor *kRS* set to a value of 0.036.

The local side radius R_{Sx} of the free side-surface calculated with Eq. 15 is plotted and shown in Fig. 14, beginning with the initial side radius R_{S0} equal to 1 mm and decreasing values along the gap

coordinate x, like it has been observed in the rolling case, the side surface is sharpened. The local minimum width b_{min} along with the gap coordinate x is shown in Fig. 15, it starts from the zero value at the inlet plane and rises to its maximum value, which is reached at the exit plane of the roll gap. With the values of the local minimum width $b_{min\,x}$ and the local side radius R_{Sx} together with the height h_x along the gap coordinate x the local area A_x can be calculated, the result is shown in Fig. 16.

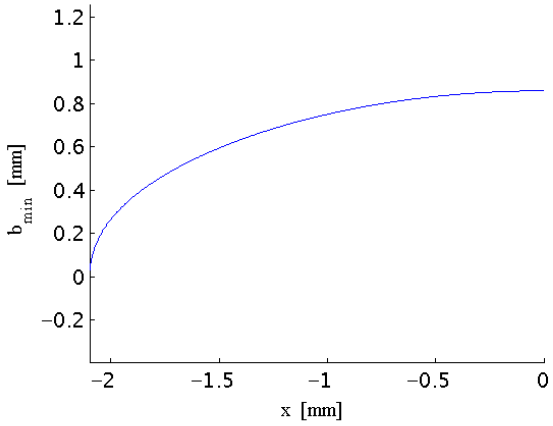

Fig. 15: Local minimum width *bmin* as a function of the gap coordinate x.

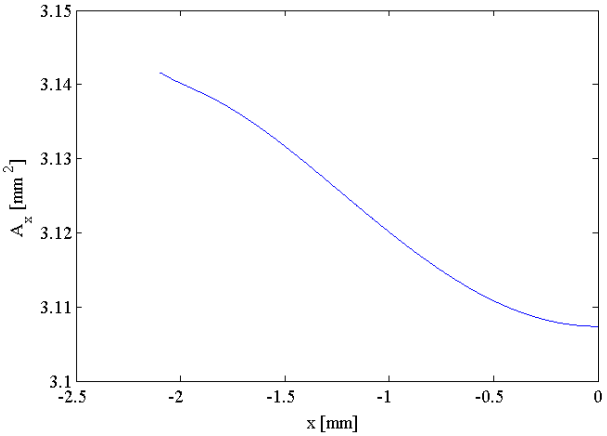

Fig. 16: Local area *Ax* as a function of the gap coordinate x.

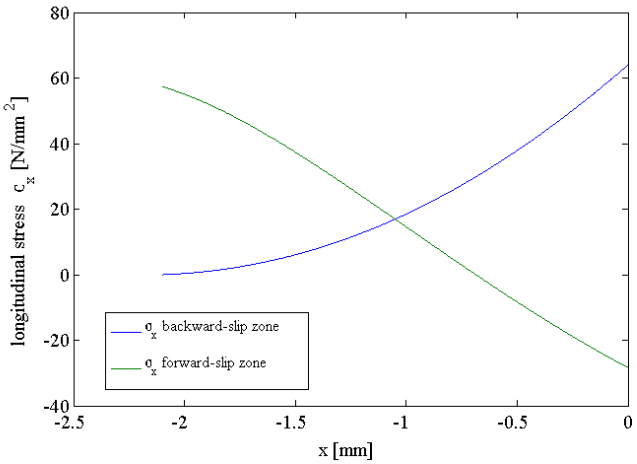

Fig. 17: Normal stress distribution σx in longitudinal direction in the forward- and backward-slip zone, with the neutral point or point of no-slip at the intersection point.

In the next step, the acting stress distributions in the roll gap are calculated. For that purpose, at first the flow stress k_f of the material described by Eq. 43 is evaluated with the locally dependent true strain φ calculated from Eq. 12. The normal stress in longitudinal direction $\sigma_x\,(x)$ is found by solving point by point the differential equation, Eq. 28, on a dense discretized point space with a numerical ODE solver. When the stress distribution $\sigma_x\,(x)$ in the forward- and backward-slip zone is found, the neutral point can be found by bringing the two solutions to intersection, see Fig. 17. By using Tresca's yield criterion, given by Eq. 27, also the normal stress distribution $\sigma_y\,(x)$ can be evaluated. The shear stress distribution $\tau_x\,(x)$ is calculated with help of Eq. 24 and Eq. 26. The friction coefficient μ_R acting between roll and wire is adjusted to the values shown in Table 5. In the combined plot shown in Fig. 18, all stresses acting along the gap can be seen.

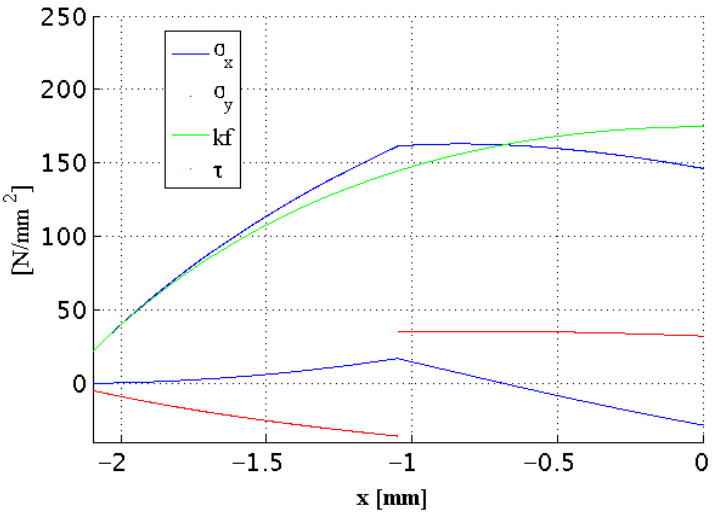

Fig. 18: Acting normal stresses σx and σy , the shear stress τx and the flow stress kf along the gap coordinate x.

With the normal stress σ_y and the local maximum and minimum width b_x and $b_{min\,x}$ the roll separating force F_{RS} is calculated from Eq. 31. By using the shear stress τ_x and the local widths, the rolling torque T_R is calculated from Eq. 32. With the help of the roll separating force F_{RS} and the acting friction coefficient μ_B in the bearing, the bearing torque T_B is calculated. From Fig. 5 the equilibrium of the acting torques can be seen. For the roll-drawing case, the shown torque of an external drive T_D has to become to zero. That case is tracked by Eq. 35. With the measured drawing force F_{Tmeas} the applied stress σ_x on the outlet of the gap has been calculated, which gave the initial condition for the stress distribution in the forward-slip zone, after that the friction coefficient μ_R has been adjusted in a way that the calculated roll separating force came as close as possible to the measured value, while the condition for having the value for the virtual torque of an external drive T_D in the ideal case exact equal to zero is more important and maintained by adjusting the friction coefficient μ_B acting in the bearing. The resulting values of the calculation and the measured ones are collected in Table 5.

Table 5: Measured and calculated forces, torques, and friction values at the contact between drawn material and rolls and in the journal bearing of the four roll-drawing passes.

$F_{RS\text{-}ms}$ [N]	$F_{RS\text{-}c}$ [N]	$(F_{RS\text{-}c} - F_{RS\text{-}ms}) / F_{RS\text{-}ms} \cdot 100$ [%]	$F_{T\text{-}ms}$ [N]	$F_{T\text{-}c}$ [N]	$T_{R\text{-}c}$ [Nm]	$T_{D\text{-}c}$ [Nm]	μ_B	μ_R
165	172	4,45	45	45	-0,26	0,0026	0,090	0,110
380	377	-0,83	88	88	-0,45	0,0052	0,090	0,220
570	571	0,13	145	145	-0,66	0,0049	0,108	0,149
865	865	-0,02	240	240	-1,04	0,0046	0,121	0,199

With the intersection point between forward- and backward-slip zone one finds the neutral point position x_N. Here, at the point of no slip, the longitudinal velocity v_x of the drawn material and the longitudinal component v_{xR} of the roll circumferential speed v_{cR} are equal, now also the neutral angle α_N can be calculated. With Eq. 36 and Eq. 37 the velocities of the wire and the roll with respect to the roll gap coordinate x are calculated. Their relation to each other can be seen from Fig. 19. The calculated maximum of the velocity difference is present at the exit plane of the roll gap, which was expected, but the absolute value of the calculated forward-slip κ is to small compared to the measured

values. The definition of the forward-slip κ is given by Eq. 38 and its graphical representation along with the roll gap coordinate x is shown in Fig. 20.

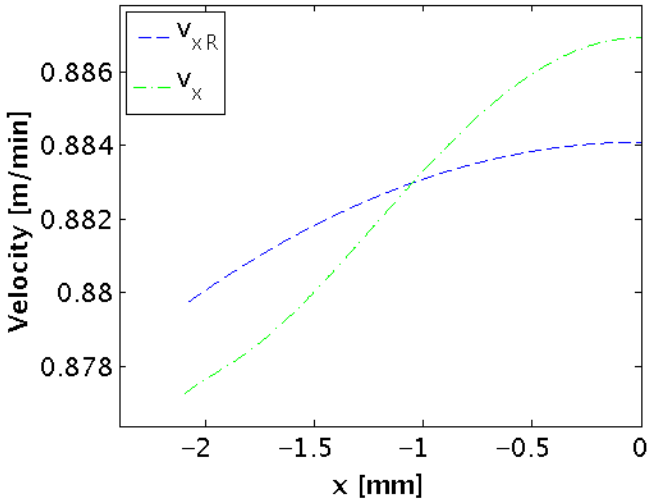

Fig. 19: Longitudinal velocity *vx* of the drawn material and the longitudinal component *vxR* of the roll circumferential speed *vcR*.

The difference between the measured forward-slip and the calculated forward-slip could be explained with a free homogeneous stretch acting on the material close to the exit plane of the roll gap, which influences also the final maximum width b_{max} to some extent. That velocity difference or mismatch is considered within Eq. 39. It is captured by an external plastic stretch λ_{ext} the wire additionally undergoes after leaving the roll gap. The measured and the calculated forward-slip values and the external stretch λ_{ext} is shown in Table 6.

Table 6: Measured forward-slip *κms* and calculated forward-slip *κc* and the calculated external plastic stretch λext acting after the roll gap.

κ_{ms} [%]	κ_c [%]	λ_{ext}
2,57	0,18	1,024
3,85	0,32	1,035
4,05	1,22	1,021
5,29	1,99	1,032

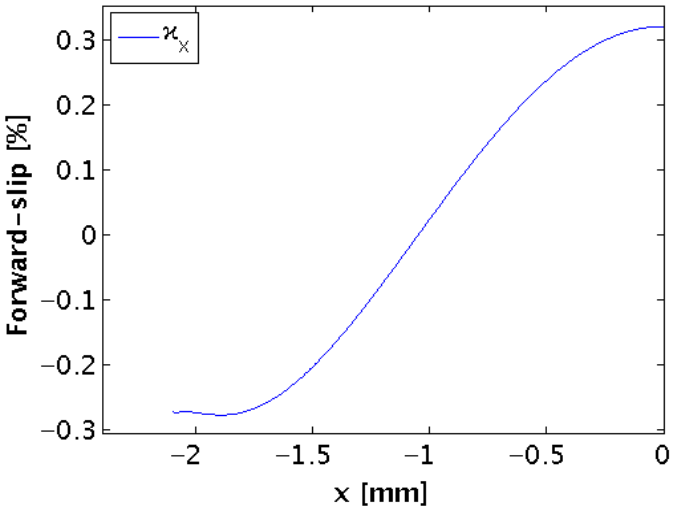

Fig. 20: Calculated forward-slip κ along the roll gap. Fig. 20: Calculated forward-slip κ along the roll gap.

With Eq. 40 the influence of that external plastic stretch onto the area of the wire which is present exactly at the exit plane of the gap is described. The area reduced by that acting plastic stretch is then taken for the calculation of a new reduced maximum width $b_{x>0}$ behind the gap, for that Eq. 41 is taken. The influence on the minimum width b_{min} is treated with Eq. 42. The results of the comparison of calculated and measured values of the maximum width b_{max} are given in Table 7. The calculated minimum width $b_{min\text{-}c}$ at the end of the gap, the minimum width calculated and the minimum width in a distance to the exit plane of the gap $b_{min\ x>0\text{-}c}$ and the minimum width measured within the close up photograph of the samples $b_{min\text{-}ms}$ and a comparison is given in Table 8.

Table 7: Measured maximum width b1-ms and calculated maximum width b1-c at the end of the gap and after considering the external stretch λext.

b_0 , h_0 [mm]	h_1 [mm]	$b_{1\text{-ms}}$ [mm]	$b_{1\text{-c}}$ [mm]	$(b_{1\text{-c}} - b_{1\text{-ms}})/b_{1\text{-ms}} \cdot 100$ [%]	$b_{x>0}$ [mm]	$(b_{x>0} - b_{1\text{-ms}})/b_{1\text{-ms}} \cdot 100$ [%]
2,00	1,88	2,02	2,03	0,65	1,99	-1,27
	1,79	2,05	2,07	0,98	2,01	-1,90
	1,69	2,09	2,12	1,29	2,07	-1,05
	1,57	2,14	2,18	1,92	2,12	-0,86

Table 8: Measured minimum width bmin-ms and calculated minimum width bmin-c at the end of the gap and after considering the external stretch λext.

$b_{min\text{-ms}}$ [mm]	$b_{min\text{-c}}$ [mm]	$(b_{min\text{-c}}-b_{min\text{-ms}})/b_{min\text{-ms}} \cdot 100$ [%]	$b_{minx>0\text{-c}}$ [mm]	$(b_{minx>0\text{-c}} - b_{min\text{-ms}})/b_{min\text{-ms}} \cdot 100$ [%]
0,58	0,63	8,58	0,59	1,87
0,79	0,86	9,29	0,80	1,78
0,90	0,95	5,24	0,90	-0,20
1,12	1,18	4,63	1,12	-0,67

The deviation between the measured maximum width $b_{1\text{-}ms}$ and the calculated maximum width $b_{1\text{-}c}$ at the exit plane of the gap shows a mean positive deviation of 1.2 % for the four investigated passes. After the consideration of the external plastic stretch λ_{ext} a quite bigger mean negative deviation of 1.27 % is found. For the minimum widths the deviations at the exit plane are all positive at a mean value of 6.94 %. The consideration of the plastic external stretch reduces the absolute mean deviation to 1.13 %. The influence of that external stretch onto the radius of the free side-surface is neglected in Eq. 41 and Eq. 42.

Conclusion and Outlook

The proposed model functions for the prediction of lateral spread in the investigated roll-drawing passes, initial round section to flat with curved side-surface and flat to flat, performs good in the examined dimension range. The formulas are not too complicated to handle and can enhance the roll pass design, especially they could be helpful for the choice of the appropriate initial wire dimension for a desired final dimension to be manufactured by the roll-drawing process. Additionally, they could be used for the rough calculation of the groove filling behavior in profiled wire drawing. The mechanical model for the prediction of roll separating force, external roll-drawing force and neutral angle shows promising results. The forces and torques are strongly dependent on the assumed friction coefficients and the minimum width, which are values not known in advance. With the proposed model equations in conjunction with the numerical values given for the prediction of the curvature radius of the free-side surface an educated guess should be possible of the roll pass designer. To come to a reliable calculation scheme over a bigger size range, more tests as well as parameter studies have to be conducted. The local area described by local maximum width, local minimum width and the position dependent curvature radius of the free side-surface should be investigated to a deeper extent. The next experiments will have also to take the high forward-slip further into focus, which lead to the proposed action of an external stretch, acting close behind the exit plane of the roll gap, and showing a remarkable influence onto the final wire geometry.

References

[1] Dietrich Jaschke, Untersuchungen zum Walzziehen von Drähten und Profilen aus metallischen Werkstoffen, 1977, Oberursel, Deutsche Gesellschaft für Metallkunde e.V

[2] Francesco Lambiase, Antoniomaria Di Ilio, Numerical and experimental investigation of process parameters effect of low carbon steel wire produced with roll drawing process, Key Engineering Materials, Online: 2011-03-28, ISSN: 1662-9795, Vol. 473, 113-120

[3] Francesco Lambiase, Antoniomaria Di Ilio, A prototypal apparatus for flat wires by roll drawing process, 2010, Proceedings of CIRP ICME 2010

[4] Horst Limant, Berechnung der Breitung beim Walzen von Flacherzeugnissen, 1964, Stahl und Eisen 84, 210 - 211

[5] Rodney Hill, Letter to A.W. McCrum, 16. November 1955

[6] Bernhardt Weyh, Lecture Script: Rechneranwendungen in der Metallurgie und Umformtechnik,2012, Duisburg

[7] M. Kazeminezhad, A. Karimi Taheri, Calculation of the rolling pressure distribution and force in wire flat rolling, 2006, Journal of Materials Processing Technology 171, 253-258